Vibrational dynamics of a $c(2\times2)$ phase induced by nitrogen adsorption on Cu(001)

E. Z. Ciftlikli,[1] L. V. Goncharova,[1,*] B. J. Hinch,[1,†] Marisol Alcántara Ortigoza,[2,†] Sampyo Hong,[2] and Talat S. Rahman[2]
[1]*Department of Chemistry and Chemical Biology, Rutgers University, Piscataway, New Jersey 08854, USA*
[2]*Department of Physics, University of Central Florida, Orlando, Florida 32816, USA*
(Received 11 August 2009; revised manuscript received 24 December 2009; published 31 March 2010)

Helium-atom scattering and density-functional perturbation theory (DFPT) calculations invoking the linear-response approximation and the pseudopotential approach have been used to study the vibrational dynamics of $c(2\times2)$-like phases produced by nitrogen-ion implantation and subsequent annealing of Cu(001) surfaces. We find that, while the $c(2\times2)$ phonon dispersion relations are different from those of clean Cu(001), neither the acoustic nor the optical surface phonon mode energies measured along both [100] and $[1\bar{1}0]$ directions are dependent on N coverage once the $c(2\times2)$ pattern is formed. We show that the dispersion of the surface phonon modes is well reproduced with an analysis of the DFPT calculations of a nonstress relieved $c(2\times2)$ structure. A marked softening of a zone center optical mode is very apparent both experimentally and in the calculations. We show this softening arises largely because of interplanar Cu surface relaxations induced by N adsorption.

DOI: 10.1103/PhysRevB.81.115465 PACS number(s): 81.07.−b, 63.20.D−, 63.22.−m, 61.46.−w

I. INTRODUCTION

The nitrogen on Cu(001) adsorbate system has received much attention in recent years, as it is a system that is known to exhibit nanoscale ordering. Large-scale superstructures, which are observed at N coverages below 0.35 ML, self-assemble with a repeat distance of order 55 Å. Essentially, nearly perfect square patches are known to assemble between narrow nitrogen-free channels aligned along [100] directions. Inside the patch, there is an ordered phase that appears $c(2\times2)$-like. A lower resolution low-energy electron diffraction (LEED) system does not distinguish the high-order superstructure from a simple $c(2\times2)$ structure.[1,2] However, LEED and x-ray diffraction have now been used successfully in resolving the larger-scale superstructure periodicity.[3–5] STM has been used by many authors to study the superstructures.[6–11] The assembly of the superstructure at lower coverages has also been traced by STM.[12] An extensive review is available.[8]

While copper nitride interfaces have some applications in interconnect technologies,[13] interest in this nanoscopic system has largely been motivated by the possibility of using it as a template for further growth of nanoscale structures. For example, oxygen adsorption on this superstructure has been shown to be site-selective.[14] Also the electronic properties of metal clusters grown on N-containing and N-free regions differ.[15] Metallic overlayer growth may be concentrated between the N-containing patches.[16–20] A particular interest, of course, has been looking into the possibility of high-density data storage by the reading and writing of magnetic information in arrays of small magnetic clusters grown on the N on Cu template.[21]

Our initial studies were motivated by an interest in the effects of stress on the dynamics of the basic $c(2\times2)$ structure. Croset and co-workers[3,5] have proposed that the large-scale assembly is due to stress relief, that is, strain compensation within the $c(2\times2)$ patches by lateral displacements in the N-free regions. Their x-ray diffraction studies have been strongly supportive of strain fields that extend many layers deep into the single-crystal Cu substrate, and that develop because of the intrinsically stressed N-containing patches. This type of strain pattern has also been employed in the analysis of "distortions" of Cu and N arrays in scanning tunneling microscopy (STM) images.[8,11] At N coverages above 0.35 ML, and approaching N saturation at 0.5 ML, stress relief is achieved by a second distinct mechanism: channels of missing Cu atoms are seen to assemble, aligned along $[1\bar{1}0]$ directions.

In the vast majority of studies it has been assumed that the $c(2\times2)$ structure has a p4mm symmetry based on N's sitting in fourfold hollow sites. However photoelectron diffraction (PhD) has indicated an alternative structure of a lower p2mm symmetry, in which the N atoms are believed to sit in hollow sites, but at a height between a split-height Cu plane. Hoeft *et al.*[22] have proposed that half of the "top layer" of Cu atoms are displaced upwards with respect to a lower half. Figure 1 illustrates the essence of the conflicting models for the $c(2\times2)$ structure. Hoeft's model has credibility, as the rumpling of the topmost Cu plane is a possible mechanism for lateral stress relief with the $c(2\times2)$ N/Cu(001) structure. However, our recent density-functional theory (DFT) calculations of the structure and surface stress on $c(2\times2)$ N/Cu(001) surface[23] have shown that the most stable 0.5 ML N/Cu(001) phase is the fourfold hollow model, as in earlier calculations of Yoshimoto and Tsuneyuki,[24] and that Hoeft's rumpling does not act to relieve the high compressive stress induced by the N atoms on the surface.

In this paper we report on recent He atom scattering (HAS) measurements of the $c(2\times2)$ N/Cu(001) structure and on the calculated vibrational modes of the relaxed but "unreconstructed $c(2\times2)$ N/Cu(001)," and compare these with prior electron-energy-loss spectroscopy (EELS) measurements. Close agreement in vibrational mode energies is found. The fourfold hollow adsorbate model is also able to predict accurately the dispersion of some newly observed optical phonon modes, seen along the Γ-Σ([100]) direction. Lastly, we seek evidence for the influence of lateral stress variations on surface phonon mode energies.

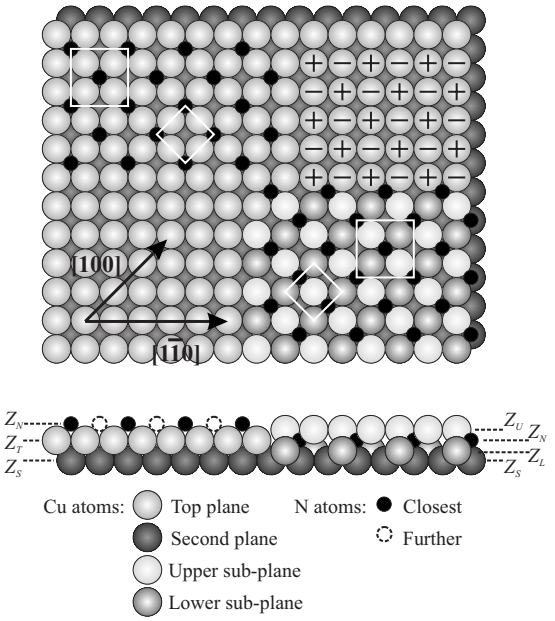

FIG. 1. Top and side views of two models for the $c(2\times2)$ local structure, observed in the N/Cu(001) adsorbate system. The two large white squares show the $c(2\times2)$ unit cell. The equivalent $p(\sqrt{2}\times\sqrt{2})R45°$ unit cells are shown with the smaller white diamonds. In the top view, the upper left quadrant illustrates the conventional fourfold hollow-site model that has been assumed by the majority of authors. The lower right quadrant illustrates the second model of Hoeft *et al.* Note that the highest copper atoms are shown in the lightest shade of gray. The second model has two different heights in the "top 1 ML Cu." The vertical displacements have been exaggerated in the side view; the heights of (sub)planes are indicated here also. The upper right quadrant, in the top view, illustrates the senses of the displacement pattern of an M-point Cu surface phonon that is equivalent to the Cu displacements seen in the second model for the $c(2\times2)$ unit cell.

II. EXPERIMENTAL METHOD

The experiments were performed in a 99.0° fixed scattering angle, high-resolution, helium atom scattering apparatus that has been described in detail elsewhere.[25] Briefly, an intense thermal-energy He beam is made by expansion of ~30–60 bar helium through a 20-μm-diameter nozzle and by separation of the emergent shock wave with a 0.5 mm skimmer. The nearly monoenergetic ($\Delta v/v\sim1\%$) He beam is scattered from the sample crystal and pulse counting is performed with an rf quadrupole mass spectrometer. Energy analysis is achieved through time-of-flight measurements. The incident energy is controlled by varying the nozzle temperature. In the measurements reported here, the incident atom beam energy varied between 14.5 and 31.5 meV. $J=0\rightarrow1$ HD rotational energy losses/gains were used to calibrate the time-of-flight path length of this instrument.[25]

In a base pressure of $<2\times10^{-10}$ mbar, the single-crystal, 1-cm-diameter Cu(001) sample was cleaned with repeated cycles of sputtering (15 min, Ne^+, 1 keV, ~13 $\mu A/cm^2$) at room temperature, and annealing up to 673 K for 10 min. The nitrogen exposure was achieved through bleeding of N_2 through the same ion gun source. The total current (including 1 keV N^+- and/or $N2^+$-ion currents) on the room-temperature grounded sample was measured to be typically of order ~5 $\mu A/cm^2$. The integrated current was used as a measure of the cumulative N implantation on or into the surface. Final sample preparation typically involved annealing to 600–620 K for 5 min. Auger electron spectroscopy was used to monitor N coverages. The normalized peak-to-peak N KLL 380 eV/Cu LMM 920 eV ratio was $\sim0.25\pm0.02$ for an annealed N-saturated surface, ($E_p=3$ kV), with 0.49 ML of N.[9] 3000 μC ion exposures were more than sufficient for N saturation. The majority of the phonon measurements, shown later, are taken from saturated surfaces at an exposure level of 5000 μC.

III. CALCULATIONAL METHOD

We have carried out density-functional theory calculations using the generalized gradient approximation (GGA) based on the plane-wave basis set and the pseudopotential approach.[26] The QUANTUM-ESPRESSO computer code[27] was used with ultrasoft pseudopotentials[28] for all elements. For the exchange-correlation energy, the GGA was used with the Perdew-Burke-Ernzerhof functional.[29] A kinetic-energy cutoff of 40 Ry was used for the plane-wave basis set. Simulations of the unreconstructed $c(2\times2)$ N overlayer on Cu(001) used a $c(2\times2)$ unit cell. A supercell consisted of a slab of nine Cu layers separated by 15 Å of vacuum. The slabs were symmetric about the center layer and thus held inversion symmetry. Integrations inside the Brillouin zone of the $c(2\times2)$ unit cell are performed according to the Monkhorst-Pack scheme,[30] with a rectangular grid of k points of dimensions $9\times9\times1$. The so-performed integrations use a Gaussian broadening technique[31] for the level occupation, where the smearing parameter is set to 0.2 eV. The N atoms were adsorbed on both sides of the slab. All atoms were allowed to relax until forces on each atom reduced to less than 2×10^{-3} eV/Å.

Surface phonon mode calculations were performed for an unreconstructed $c(2\times2)$ N/Cu(001) phase. Namely, calculations were made for an infinitely extended, nonstress-relieved, $c(2\times2)$ phase. We have used density-functional perturbation theory (DFPT) calculations based on linear-response theory and the harmonic approximation.[32,33] Phonon dispersion curves were obtained by a standard Fourier interpolation method using a (2×2) q-point mesh. Surface force constants were merged with bulk force constants and an asymmetric bulk slab of 45 layers was added to obtain projected bulk phonon modes using standard lattice dynamical methods.

Vibrational modes were labeled as "surface modes" when the eigenvectors contained contributions larger than 30% within the top two Cu layers.

IV. RESULTS AND DISCUSSION

We have used helium scattering to measure phonon modes of the $c(2\times2)$ N/Cu(001) surface, along both [1$\bar{1}$0] and [100] azimuthal directions. EELS studies of surface phonon modes in this surface as measured along the [1$\bar{1}$0] di-

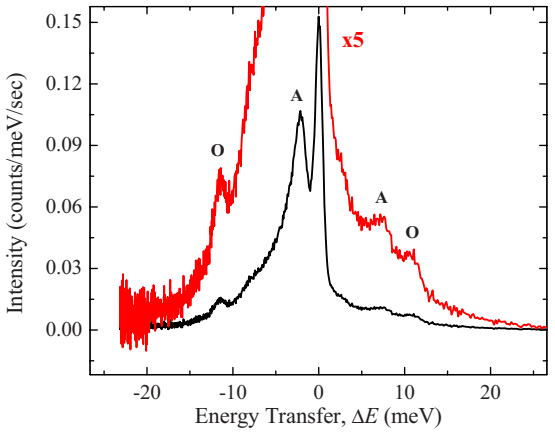

FIG. 2. (Color online) Energy-resolved helium-atom backscattered intensities, measured at an incident angle, θ_i=47.5°. The total scattering angle is fixed at 99.0°. The incident-beam energy E_i =31.3 meV, and incident azimuth [100]. N-ion exposure =5000 μC, Θ_N=0.49 ML. The surface temperature T_x=300 K. The letters "A" and "O" on the graph refer, respectively, to acoustic and optical modes.

rection, i.e., from Γ through to the X point of the Brillouin zone, have already been reported.[34,35] Unfortunately data had not been included for the other, [100], high-symmetry direction. The helium scattering data here complements this data, and also shows new results in the Γ-M direction. An energy-analyzed He-atom scattering scan is illustrated in Fig. 2. The single peaks are indicators of the diffuse elastic scattering component along this direction (at ΔE=0) or of discrete energy transfers to/from surface phonon modes. At this angle, four distinct inelastic peaks are resolved.

Information from this and many similar time-of-flight scans are used to compound the information in the surface phonon dispersion plot of Fig. 3. In the extended zone scheme both acoustic and optical modes are observed, and the intensities of these modes are seen generally to die away with increasing exchange of parallel momentum. The acoustic mode is probably a Rayleigh-type mode, involving strong perpendicular displacements of the copper atoms along a surface normal. Assignment of the optical mode is best done by comparison with the calculated phonon mode energies.

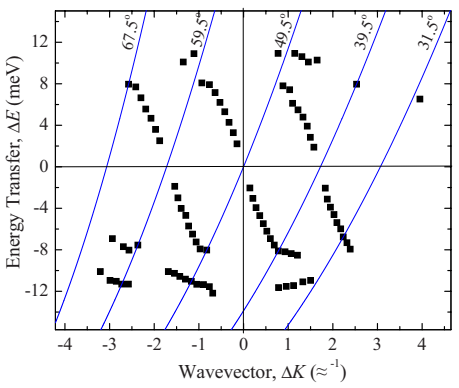

FIG. 3. (Color online) Dispersion curves of measured surface-phonon modes, along the [100] azimuth and plotted in the expanded zone scheme. Example scan curves (continuous parabolas—blue in the color online version) are illustrated to indicate the extent of scattering angle used; θ_i=29.5°–67.5°. E_i=31.3 meV, incident azimuth [100], N exposure=5000 μC, Θ_N=0.49 ML, and T_x =173 K.

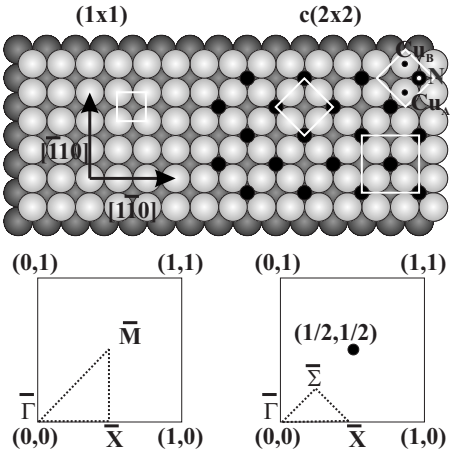

FIG. 4. Real-space images of the (1×1) Cu surface and the $c(2\times2)$ N on Cu structures are shown above. Note: the $c(2\times2)$ is equally described as a $p(2\times2)R45°$ unit cell. Reciprocal lattice points, especially those at high-symmetry positions, are illustrated in the lower row.

The presence of an optical mode is not surprising as it can be thought of as a backfolded mode, following the ordering of the N adsorbate and enlargement of the surface unit cell to the $c(2\times2)$ structure. Figure 4 illustrates the nature of the reciprocal lattice backfolding, in an ideal $c(2\times2)$ structure, and defines the terminology used here for high-symmetry reciprocal lattice points.

By backfolding the Σ-M surface phonon modes, the phonon dispersion data can be summarized in the reduced zone dispersion plot of Fig. 5. Note that these data utilize an incommensurate reciprocal lattice vector=1.700 Å^{-1}. This value was selected as a means to map all modes from first, second, and even the third Brillouin zones on to a single

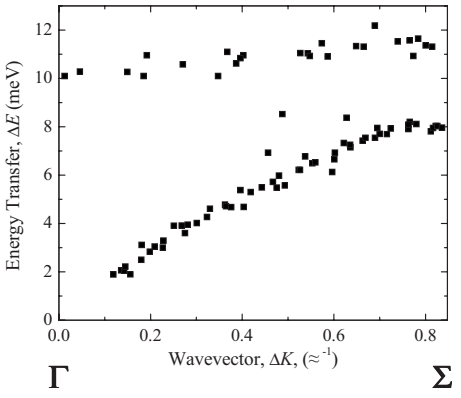

FIG. 5. Dispersion curves of measured surface-phonon modes, plotted in the incommensurate reduced zone scheme along the [100] azimuth. E_i=31.3 meV, N exposure=5000 μC, Θ_N=0.49 (~0.5) ML, and T_x=173 K. Note: in the backfolded scheme a 2.4% expanded lattice parameter of 3.696 Å is utilized to map one dispersion curve onto itself. The zone boundary position is found at 0.850 Å^{-1}. The corresponding bulk value is at 0.870 Å^{-1}.

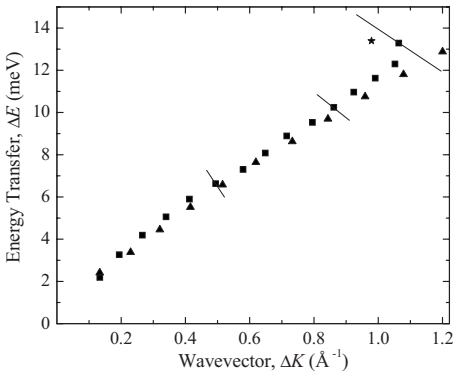

FIG. 6. Dispersion curves of measured surface-phonon modes along the $[1\bar{1}0]$ azimuth. E_i=31.3 meV, N exposure=5000 μC, Θ_N=0.49 ML, and T_x=173 K. Triangles designate peak positions originating from positive-energy transfer to the He atom upon scattering. Squares represent observed peak positions of modes with negative energy transfers. Short lines show sections of scan curves; their lengths represent the FWHM of the observed phonon features. The star is the weakest feature observed one which is distinctly removed from the main Rayleigh-type mode features.

curve. Modes detected along the $[1\bar{1}0]$ high-symmetry direction (Γ-X) are plotted in Fig. 6. All these modes are taken from the first zone only; the incommensurate zone boundary is anticipated to be at 1.202 Å^{-1}, Fig. 7(a) shows how our calculated full dispersion of surface and near-surface phonon modes of the optimized unreconstructed $c(2\times2)$ N/Cu(100) phase compares with our experimental data.

Before analyzing these calculations, it is useful to test the computational techniques by applying them to the clean surface. Figures 7(b) and 7(c) show how the calculated dispersion curves compare with early experimental data. Likewise, key "high-symmetry point" clean-surface mode energy estimates are reported in Table I below and compared with previously reported measurements. The clean-surface Cu(001) has been studied extensively by theory and experiments (see Refs. 39–41 and references therein). Of particular relevance to the present calculation is that of Dal Corso, who analyzed at length the phonon dispersion of clean Cu(001) by also using the density-functional perturbation theory with the generalized gradient approximation (with the Perdew-Burke-Ernzerhof functional), the plane-wave approach, the pseudopotential (ultrasoft) scheme, and the QUANTUM-ESPRESSO computer code. The agreement between DFPT calculations and phonon measurements has been, in general, fairly satisfactory. The sharp longitudinal resonance detected in HAS measurements[38] on Cu(001), however, has not so far been reproduced in DFPT calculations. In the present paper we shall not address the answer to the origin of such a longitudinal resonance, partly because it is not present in our HAS spectra after N chemisorption. However, since the issue of the longitudinal resonance has been a long-standing problem that persists for several metal surfaces, we refer the reader to the work of Chis *et al.*, who recently addressed the cases of Al(001) (Ref. 42) and Cu(111).[43]

Since in the following analysis we also describe how the modes of clean Cu(001) change upon N chemisorption, it is thus instructive to compare the phonon mode energies of the unreconstructed $c(2\times2)$ N/Cu(100) phase with those from the clean (N-free) surface. High-symmetry point mode energies from calculations of the idealized and unreconstructed $c(2\times2)$ structure can be compared with experimental observations and estimates from a clean surface in Table II following.

Many of the dispersion curves in Figs. 7(a)–7(c) fade out at certain points in the Brillouin zones as, when surface and bulk modes of mixable symmetries approach resonance, the displacement patterns may become more extensively distributed throughout the slab. The mode polarizations can also change across the zone. For the N/Cu system, and in both Γ-X and Γ-Σ phonon directions, close agreement is found between measured and some calculated phonon energies. Thus, for almost all observed modes we are able to unambiguously identify the polarization vectors. Below we discuss these mode polarizations for the observed dispersion modes and for selected other modes.

Along the Γ-Σ([100]) direction, predominantly only clean-surface Rayleigh-type waves are observed via helium scattering. In practice, cross-sections of the other (calculated) vibrational modes are too low for observation. The presence of the N overlayer with $c(2\times2)$ periodicity induces a gap opening of the old (clean-surface) Rayleigh wave. The displacement patterns of the new zone boundary modes, at Σ, are illustrated in Fig. 8. Both show vertical displacements within the topmost Cu layer, and longitudinal and vertical motions within the second layer Cu atoms. Only the lower "8.9 meV" mode exhibits vertical motion of the N atoms as well.

We now explain why the presence of adsorbed N will induce a gap opening at Σ. Without N, the two substrate displacement patterns in Figs. 8(a) and 8(b) are identical. Given the displacement patterns in the presence of N, however, there are two nonequivalent sites for N: (1) above the second-layer Cu atoms that have vertical displacement [Fig. 8(a)] and (2) above the second-layer Cu atoms that have horizontal displacement [Fig. 8(b)]. Due to N-site occupation, the modes in Figs. 8(a) and 8(b) lose degeneracy and a splitting of $\gtrsim$2 meV is induced.

All Γ-Σ modes have p2mm-symmetry displacement patterns. At the zone boundary, the first layer couples only to the longitudinal motion of the second layer. Between Γ-Σ points, both longitudinal and vertical displacements are seen to some degree in both first and second layers. The HAS technique has mapped out a continuous dispersion curves in the Γ-Σ direction (see Fig. 5). The observed optical phonon mode branch runs from between 10.0 ± 0.3 meV (8.4 meV in the calculations) at the zone center to 10.8 ± 0.3 meV (10.8 meV in the calculation as well) at the zone boundary (Σ).

The calculations indicate that there is an additional surface mode that is located above the observed optical mode branch. At Σ it has a frequency of 14.3 meV. This mode is of pure shear-horizontal polarization and is not able to couple to the vertical optical mode nor is it expected to be excited by helium-atom scattering along this high-symmetry direction (He scattering cannot pick up pure shear-horizontal modes). HAS has seen evidence of another distinct mode, observed only in the second zone, dispersing away from the lower

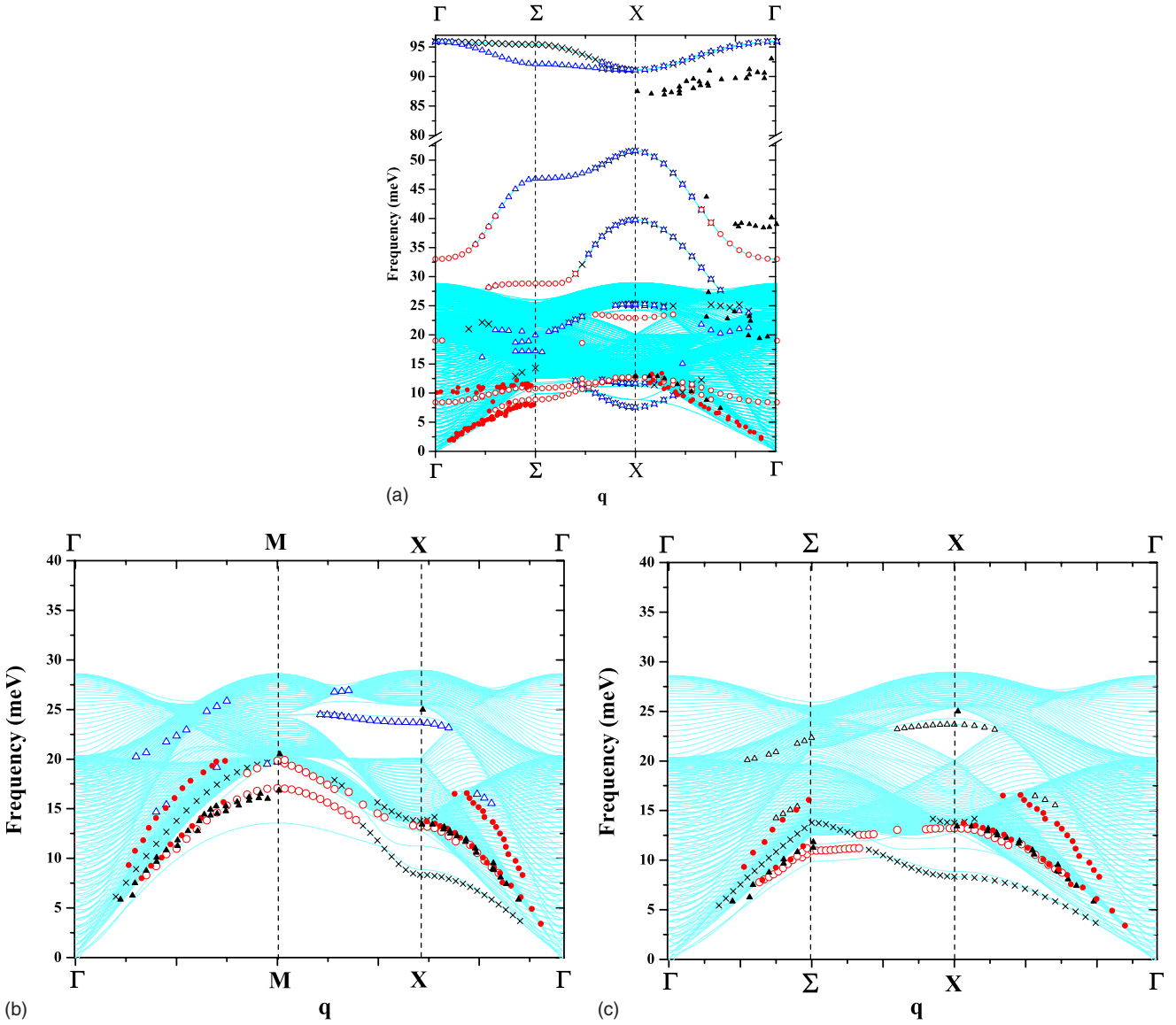

FIG. 7. (Color online) Calculated surface-phonon dispersion curves (a) for the unreconstructed $c(2\times2)$ N/Cu(001); (b) and (c) for clean Cu(001) along two different direction sets: (b) along ΓMX directions and (c) along ΓΣX directions. q denotes the surface parallel momentum of calculated modes; cf. with experimental ΔK values. Projected bulk modes are depicted as solid lines in background. Surface modes are depicted as circle (vertical polarization), triangle (longitudinal mode), and cross (shear-horizontal mode). Note that only major polarizations are shown, namely, for weight ≥30% in the top two Cu layers. Filled (red) circles and (dark) triangles represent HAS and EELS (Refs. 35 and 36) data, respectively.

mode that has a frequency of 8.1 meV at the zone boundary. Yet, given our calculated displacement patterns, neither of the perpendicularly polarized high-symmetry-point Σ modes is expected to be twofold degenerate.

The observed optical mode of the reciprocal lattice unit cell (Γ-Σ) has a sense of dispersion that is opposite to that anticipated for simple backfolding of the Cu Rayleigh mode. The energy, $\sim 10.0 \pm 0.3$ meV, of the mode at the Γ point appears to be substantially reduced compared to that of the M-point Rayleigh phonon on a clean Cu(001) face at 16.8 meV.[38] This M-point mode has the same Cu displacement pattern that was considered in the structural model of Hoeft *et al.*, illustrated in Fig. 1 above. The stress-relief mechanism they propose to occur within the uniformly compressed N/Cu overlayer could be, in part, responsible for the softening of this vibrational mode. However, for three fundamental reasons, we think this is not the explanation. First, the number of observed phonon modes, with perpendicular polarization, is not consistent with the rumpled model. For every perpendicularly polarized mode seen in the Γ-Σ direction in a p4mm surface (the N in fourfold hollow model), a lower symmetry p2mm surface (as per Hoeft's model) must exhibit two nondegenerate perpendicular modes. Except for the zone center, the two domains would give rise to two distinct modes. A surface rumpling might limit the range of observation of some modes with He scattering, especially close to Σ, but we cannot state that we observe two distinct mode branches dispersing from the Γ point. Second, we have looked explicitly for a surface temperature dependence of surface phonon mode energies. (A soft mode could give rise

TABLE I. Energies of surface phonons at high-symmetry points for the clean Cu(001) surface. Our calculated mode energies (GGA) are compared with the experimental values from earlier EELS (Ref. 37) and HAS data (Ref. 38). The mode descriptors have a format $\{V|L|H\}^i$ in the descending order of vibrational weight, where *i*, V, L, and H are mean-layer index, vertical, longitudinal, and shear-horizontal polarizations, respectively.

		Mode energies (meV)		
BZ	Mode descriptor	GGA	EELS	HAS
M	V^1	17.1	16.7–16.9	16.8
	L^1L^2	19.7	20.5	
	H^1H^2	19.7		
	V^2	19.9	20.5	
Σ	$V^1V^2L^1L^2$	10.9	11.0–11.9	12.0
	$V^1V^2L^1L^2$	11.6	11.0–11.9	
	H^1H^2	13.8		
	$L^1V^1L^2V^2$	15.9	16.6	16.6
	L^2V^1	22.3		
	$V^2L^2V^1L^1$	24.2		
X	H^1	8.3		
	V^1L^2	13.2	13.4–13.6	13.8
	H^2	13.8		
	L^1V^2	23.7	25.2	

to a locked-in top-layer rumpling.) In helium scattering, we have not discerned any temperature dependence between 173 and 300 K of any observable modes. Significantly, the Γ-point mode energy does not vary in such a way as to indicate an imminent or an established symmetry lowering of the N/Cu(001) phase as might have been expected for introduction of a Hoeft-type Cu layer rumpling. And third, our calculations on the stress level of $c(2\times2)$ N/Cu(001) have suggested that the surface stress within the $c(2\times2)$ N/Cu(001) is not effectively/adequately relieved with the addition of the proposed rumpling displacements within the first-layer Cu atoms.[24] We thus conclude that surface rumpling is not the cause for the softening of this Γ-point optical mode. More importantly, perhaps, when we carried out calculations for Hoeft's model at saturation coverage it turned out to be energetically unstable. That is, such a rumpled structure relaxes toward the unreconstructed surface that we describe in this work. Furthermore, we found that even the slightest rumpling on the first layer renders the system dynamically unstable, a condition that makes the model physically implausible.

In fact, the predominant cause for the softening of the Γ-point vibrational mode is the effect of N on the layer 1 to layer 2 interlayer spacing. The calculated force-constant matrix demonstrates this effect. Since the mode contains purely vertical vibration of the first Cu layer only (that is, 100% of the displacement weight is in the first layer), only vertical force constants of the first layer Cu atoms, Φ_{ZZ} (Cu layer 1, N or Cu layer $\boldsymbol{l}$, where $\boldsymbol{l}=1,2,\ldots$) determine the frequency of this mode. However, since the force constant Φ_{ZZ} (Cu layer 1, N or Cu layer $\boldsymbol{l}$) decreases exponentially with the bond length, it is clear that the interactions with nearest neighbors in the first layer or second layer or the interaction of first layer Cu with the N overlayer are most significant. All other interactions contribute considerably less. Table III shows the calculated force-constant matrix elements for these interactions in the clean and in the N-containing Cu(001) surface. The *interlayer* force constant Φ_{ZZ} (Cu layer 1, Cu layer 2) is the largest. Table III indicates that with $c(2\times2)$ N coverage the Φ_{ZZ} (Cu layer 1, Cu layer 2) force constant is reduced by as much as 40%. This change is supplemented by a smaller absolute change in the intralayer Φ_{ZZ} (Cu layer 1, Cu layer 1) but is slightly mitigated by introduction of a negative Φ_{ZZ} (Cu layer 1, N) element with N adsorption. The large softening of the mode at the M point, with N coverage on Cu(001) is thus dominated by the N-induced relaxation, i.e., an 8% expansion of the spacing between Cu layer 1 and 2 and the associated force constant reduction.

At Γ other normal modes of the N/Cu(100) surface arise with considerable near-surface displacement amplitudes. Specifically, a V^2 mode shows in the calculations at ~19.0 meV. Calculations show an $N^{\perp}$ mode at 33.0 meV. No Γ-point in-plane (longitudinal or H type) modes are identified at all in the calculations until the $N\|H^1L^1$ mode(s) at 95.9 meV. Modes with longitudinal (L^1) character are observed only midway and beyond in the Γ-Σ direction. At Σ the L^1 mode is found at 17.2 meV.

The addition of N to the structure enlarges the unit cell, and the new $[1\bar{1}0]$ mirror planes now run through N-containing sites (and no longer through planes containing the top-layer Cu atoms). That is, not all Cu atomic core positions are centered on mirror planes. Thus, in contrast to what happens on an adsorbate-free Cu(001) surface, where every atom lies on a mirror plane, phonon modes along the $[1\bar{1}0]$ directions are no longer required to be purely odd or even with respect to the $[1\bar{1}0]$ plane. In other words, not only shear vertical and longitudinal displacements may couple but now also the "shear-horizontal" modes can all couple together. Indeed a (H^1L^1) phonon mode of 7.5 meV is found at the X point containing both shear-horizontal and longitudinal components. This and other selected X-point phonon modes are illustrated in Fig. 9.

Interestingly, the 7.5 meV "clock" displacement pattern is one that is believed to lock in on the C/Ni(001) face. On the latter face a $p(2\times2)$ superstructure is formed, at 0.5 ML of carbon in fourfold hollow sites, with the locked-in soft-clock-mode p4g-symmetry reconstruction. The clock-mode displacements do not involve approach of top-layer Cu atoms toward N centers. Consequently, Ibach and co-workers[45,46] were able to show that the energy of this mode can approach zero if a force constant between first and second Cu layers approaches zero. In addition, the N-Cu distances are, in fact, increased slightly by the radial, clock-type motion about N centers. Thus, Müller *et al.*[47] argued that a soft-phonon mechanism for reconstruction could be induced by a large compressive stress, such as is present in C/Ni(100). (The clock mode was not expected to be driven to zero energy in a surface of this symmetry, i.e., one under tensile stress.)

TABLE II. Energies of surface phonons at high-symmetry points for the $c(2\times2)$-N/Cu(001) surface. Our calculated mode energies (GGA), for the optimized N in fourfold hollow-site structure, are compared with the "best guess" experimental mode assignments of the reported EELS data, Refs. 34–36 and 44, and our HAS data set.

		Mode energies (meV)			
BZ	Mode descriptor	GGA	EELS	HAS	Clean-surface mode for comparison
Γ	V^1	8.4		10.0	17.1 (V^1) at M
	V^2	19.0	19.2[a]		19.9 (V^2) at M
	$N^{\perp}V^2$	33.0	38.5[a] 40.2[b]		
	$N\|\|H^1L^1$	95.9	91.7[c] 93.0[d],[e]		
	$N\|\|L^1H^1$	95.9	91.7[c] 93.0[d],[e]		
Σ	$V^1V^2L^2N^{\perp}$	8.9		8.1	10.9 ($V^1V^2L^1L^2$)
	$V^1V^2L^2N\|\|$	10.8		10.8	10.9 ($V^1V^2L^1L^2$)
	$H^2H^1N\|\|$	14.3			
	L^1L^2	17.2			15.9 ($L^1V^1L^2V^2$)
	$L^2L^1V^1V^2$	19.9			
	$L^2V^2L^1V^1$	20.8			
	$N^{\perp}L^1V^2L^2$	28.8			
	$L^1N^{\perp}V^2$	46.8			
	$N\|\|$	92.1			
	$N\|\|H^1$	95.4			
X	H^1L^1	7.5			8.3 (H^1)
	L^2V^1	11.6			
	H^2V^1	11.6			
	V^1L^2	12.8	13.0[f]	12.5	13.2 (V^1L^2)
	V^1H^2	12.8	13.0[f]	12.5	13.8 (H^2)
	$N^{\perp}V^2H^1L^1$	22.9			23.7 (L^1V^2)
	L^2V^1	25.1			
	H^2V^1	25.1			
	H^1L^1	25.3	25.7[g]		
	H^1L^1	39.7			
	$H^1L^1N^{\perp}$	51.6			
	$N\|\|$	91.1			
	$N\|\|$	91.1			

[a]Vertical mode (Ref. 36).
[b]Unknown polarization (Ref. 44).
[c]In-plane mode (Ref. 35).
[d]In-plane mode (Ref. 36).
[e]Vertical mode (Ref. 44).
[f]Vertical polarization (Rayleigh wave) (Ref. 35).
[g]Unknown polarization (Ref. 36).

For a surface that is under compressive stress, the clock mode might approach zero energy even with a finite interaction with lower lying layers. In the case of N/Cu(001), a reduced interaction between top-layer and second-layer Cu atoms is implied because the calculations render an N-induced 8% interlayer expansion. Yet, even taken together, the apparent interlayer expansion and the calculated compressive stress appear insufficient to invoke the $p(2\times2)$ clock-mode reconstruction here. Furthermore, the local minimum in vibrational mode energies at the X point (i.e., for the clock mode) does not necessarily imply any substantial softening of that mode. Rather, it is simply the result of backfolding of the X-M surface phonon mode in Fig. 7(b) onto the X-Γ direction. Figure 4 illustrates the nature of the reciprocal lattice backfolding. The 7.5 meV mode can also be considered as a linear combination of the star of four equivalent X-point shear-horizontal modes, umklapped into the same reciprocal lattice point. In fact the calculated 7.5 meV clock-mode energy is scarcely affected by backfolding; compare this 7.5 meV with the 8.3 meV ($\mathbf{H^1}$) mode of the clean surface!

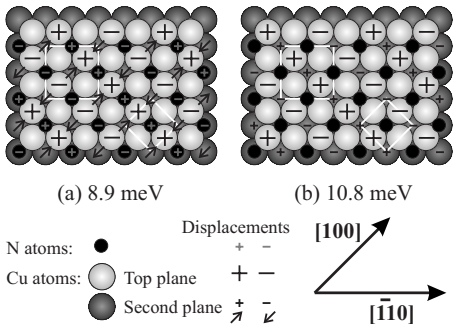

FIG. 8. Schematic displacement vector patterns, and calculated mode energies, for selected Σ-point phonon modes. Both modes involve perpendicular motion of top-layer Cu atoms and longitudinal motion of second layer atoms. (a) The 8.9 meV acoustic mode corresponds well with an experimentally observed mode at 8.1 meV. (b) The energy of the calculated "10.8 meV" optical mode agrees absolutely with an experimentally observed mode.

Three (7.5, 25.3, and 39.7 meV) of the five surface-localized X-point phonon modes, displayed in Fig. 9, exhibit combined longitudinal and shear-horizontal character in the topmost Cu layer. For example, consider the 7.5 meV mode, described as the clock-mode motion, that [on C/Ni(001)] gives rise to a p4g-symmetry reconstruction. Because of the glide plane within this displacement pattern, this mode necessarily shows zero intensity at the X point. (cf. the static diffraction pattern of the nonrealized $p(2\times2)$ p4g locked-in reconstruction.)

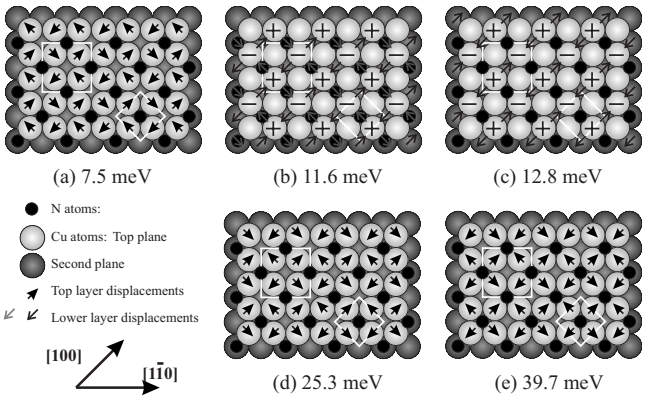

FIG. 9. Schematic displacement vector patterns, and calculated mode energies, for selected X-point phonon modes. All modes involve motion of top-layer Cu atoms. Modes at 11.6 and 12.8 meV exhibit vertical motion in the topmost Cu plane. Modes at 7.5, 25.3, and 39.7 meV have both longitudinal and shear-horizontal motion in the topmost Cu plane. The 11.6 meV mode alone displays lateral motion of the second-layer Cu atoms situated below N adsorbates. (For all modes shown here, N has comparatively small displacement vectors.) He scattering data implies the "12.8 mode" lies closer to ~12.5 meV.

TABLE III. Force-constant matrix elements $\Phi_{\alpha\beta}$ for Cu atoms in the top layers and in the presence of an N overlayer compared with those for clean Cu(001). Numerical values are expressed in dyn/cm, (1 dyn/cm=10^{-3} N/m).

	$c(2\times2)$ N				Clean				
	$\Phi_{\alpha\beta}$ (Cu layer 1, Cu layer 1)					$\Phi_{\alpha\beta}$ (Cu layer 1, Cu layer 1)			
	$\alpha\beta$	X	Y	Z		$\alpha\beta$	X	Y	Z
1NN	X	−14721.5	−17900.9	1180.5		X	−10883.7	−12088.6	0
	Y	−24660.8	−14721.5	199.7	1NN	Y	−12088.6	−10883.7	0
	Z	−199.7	−1180.5	3052.4		Z	0	0	−1477.7
	$\Phi_{\alpha\beta}$ (Cu layer 1, Cu layer 2)					$\Phi_{\alpha\beta}$ (Cu layer 1, Cu layer 2)			
	$\alpha\beta$	X	Y	Z		$\alpha\beta$	X	Y	Z
1NN	X	−3977.75	0	4568.9		X	−14776.1	0	16062.4
	Y	0	−1843.75	3425.6	1NN	Y	0	221.8	0
	Z	8441.35	2947.4	−8443.5		Z	14821.4	0	−14096
	$\Phi_{\alpha\beta}$ (Cu layer 2, Cu layer 3)					$\Phi_{\alpha\beta}$ (Cu layer 2, Cu layer 3)			
	$\alpha\beta$	X	Y	Z		$\alpha\beta$	X	Y	Z
1NN	X	−10191.8	0	13834.3		X	−12038.1	0	13101.6
	Y	0	196.1	0	1NN	Y	0	−293.2	0
	Z	12322.5	0	−12556.6		Z	12822.2	0	−12418.9
	$\Phi_{\alpha\beta}$ (Cu layer 1, N overlayer)								
	$\alpha\beta$	X	Y	Z					
1NN	X	−198676	0	27956.7					
	Y	0	2195.3	0					
	Z	13097.2	0	−2988.5					

Standard planar scattering methods are insensitive to shear-horizontal displacement components, but the scattering probe can still couple to the longitudinal motion within this layer. The 11.6 meV mode is, in principle, observable at the X point, but has only comparatively small vertical motion in the top layer. The mode is located predominantly in the second layer of atoms. (Hence it is not observed readily in the HAS measurements.) Conversely, the 12.8 meV mode is predominantly located in the first layer of Cu atoms and is more prominent at the X point. Both the "11.6 meV" and the "12.8 meV" mode displacement patterns show twofold, c2 mm symmetry but on a fourfold substrate. Thus, these modes are each twofold degenerate. This degeneracy is lost as one probes along the X-Γ direction.

The 22.9 meV X-point mode (see Table II), located mostly in the second atomic layer, shows vertical character in the second layer and, (like the 7.5 meV mode) combined longitudinal and shear-horizontal character in the first layer. The latter displacement pattern would establish a $p(2\times2)$ unit cell with p4mm symmetry. Consequently, this mode is, in principle, observable at the X point; although neither HAS nor EELS has seen such a high-lying mode. (This mode is onefold degenerate.) In contrast, another X-point surface mode with combined longitudinal and shear-horizontal character in the first layer, identified as the 25.3 meV mode, has been observed in EELS.

The 25.1 meV X-point mode involves vertical motion in the first layer and has in-plane character in the second layer. As this degenerate mode is mainly second-layer vibration, it is also not observed with HAS.

In agreement with earlier EELS data,[35,37] the energy of a mode at the X point in the surface Brillouin zone is insensitive to N addition. [EELS gives 13.4 meV (Ref. 37) for clean and 13.0 meV (Ref. 35) for N/Cu] The calculated mode is lowered only from 13.2 to 12.8 meV. He scattering sees this mode, apparently shifting with N adsorption from 13.2 to 12.5 meV. As there is as slight discrepancy between EELS and helium data, it may be that the He scattering is also slightly more sensitive to the 11.6 meV mode, as shown in Fig. 9(b). The vertical amplitude of the topmost Cu plane is of order six times smaller for the lower energy mode. The helium scattering is rarely able to resolve more than one mode, at any point along the dispersing mode from Γ to X. Close to the zone boundary we propose that the four available nondegenerate modes dispersing from X toward Γ can play a role. Some of those modes are anticipated at energies in excess of the observed 12.5 meV zone boundary energy. The experimental energy widths [full width at half maximum (FWHM)] of selected modes are also illustrated in Fig. 6. At a parallel momentum transfer ~0.9 of the way to the zone boundary (X), the FWHM of the observed 12.5 meV mode is 3.2 ± 0.3 meV. At a parallel momentum transfer ~0.9 of the way to the zone boundary, the FWHM of the observed modes is smaller, at 2.8 ± 0.2 meV. At parallel momentum transfers ~0.7 of the way to the zone boundary, or smaller, the indicated FWHM of the observed modes reduces to $\sim1.3\pm0.1$ meV. Away from zone boundary, there is another slightly unexpected result. The observed albeit "combined" modes show an almost linear dispersion. At 0.6 $Å^{-1}$ (~0.5 of the zone boundary) HAS sees a mode at ~7 meV. In contrast the calculations predict the lowest observable mode at an energy in excess of 8.5 meV. The calculated figure lies significantly outside of the HWHM of observations.

Although the energies, 12.8 and 7.5 meV, of the X-point modes were *not* strongly affected by N adsorption, there are modes that *do* undergo drastic stiffening. The strongly dispersing mode, located just above the bulk background in Fig. 7(a), is such a mode. It has a vibrational energy of 28.8 meV at Σ and 39.7 meV at X. Because there is no similar Cu(001) mode, this is a clear example of N-induced stiffening. The mode character also changes abruptly from Σ to X. At Σ it shows N, and second layer Cu, vertical displacements together with longitudinal displacement of the first-layer Cu atoms. On approaching X, it becomes a mode of purely in-plane motion of the first-layer Cu atoms. Near Γ the mode becomes resonant with bulk modes. The displacement pattern at X is of particular importance and is depicted in Fig. 9(e). The lateral motion of the top-layer Cu atoms is such that each N is simultaneously compressed by the approach of four nearest-neighbor Cu atoms. For this motion, the force constants $\Phi_{\alpha\beta}$ (Cu layer 1, Cu layer $\boldsymbol{l}$) (α,β=X,Y and $\boldsymbol{l}$ =1,2,…) and $\Phi_{\alpha\beta}$ (Cu layer 1, N overlayer) (α,β=X,Y) contribute in determining the mode energy. From the force-constant matrix we see this motion's largest force constant, Φ_{XX} (Cu layer 1, N overlayer), is 1.9×10^5 dyn/cm, which is almost an order of magnitude larger than even the largest of the first-layer Cu-Cu interatomic force constants such as Φ_{YX} (Cu layer 1, Cu layer 1). This mode, therefore, is extremely sensitive to the N addition; at the X point the resulting frequency reaches as high as 39.7 meV. Not only this mode but also those surface modes with similar in-plane polarization, such as the mode of 51.6 meV at X, show such dramatic stiffening. In contrast, in the X-point clock mode at 7.5 meV [Fig. 9(a)] the N-Cu bond-length change is second order in displacement amplitude, as the relative motions are tangential to the N-Cu line. The largest force constant of the clock-mode energy is, therefore, 2.4×10^4 dyn/cm [Φ_{YX} (Cu layer 1, Cu layer 1)] and the clock-mode energy is basically insensitive to N addition. EELS do not see this mode since its cross-section is quite small because it is a coupled shear-horizontal and longitudinal mode.[35] In regard to N vibrational modes lying above this mode, our calculated N-vibrational frequency along Γ-X shows a deviation of about 5 meV from the EELS data.

We comment now on the arguments brought forward in support of the Hoeft model.[7] The model was initially proposed on the basis of interpretation of photoelectron diffraction data.[22,48] Since then, several papers have discussed how STM images may or may not be compatible with lower symmetry phase proposed in the Hoeft model.[7,11,48–51] The issue essentially was: what does the STM, in fact, image? If the high spots in an STM image are N atoms, then the p4mm $c(2\times2)$ model is supported (with N in fourfold hollows). If instead the high spots are Cu atoms, then the second c2 mm, $c(2\times2)$ model is supported (with a rumpled Cu plane, as described by Hoeft[22]). The registry of high spots in STM, with respect to those in adjacent $c(2\times2)$ patches, is not conclusive. The registry of high spots with respect to the Cu placements is not immediately interpretable, inasmuch as the copper lattice is known to be markedly distorted at the edges

of $c(2\times2)$ patches.[5] A recent and careful work of Ohno *et al.*[11] has shown the most convincing argument for the traditional "fourfold hollow adsorption site," with N at high points in the STM image. Nevertheless, others propose alternative assignments of features in STM images—e.g., N at low points in the image.[52]

An additional argument for the "rumpled" model was based on the fact that there appear to be two types of clean "channels" between adjacent $c(2\times2)$ patches in STM images. One appears narrow, well ordered, and straight. The second is comparatively broad and meandering. Driver *et al.*[48] argued that the lower twofold symmetry of the rumpled patches automatically gives rise to the two channel types. But this argument is insufficient as, in practice, two channel types can exist without involving the lower symmetry $c(2\times2)$ structure. Specifically, adjacent p4mm $c(2\times2)$ regions that exist with one N-placement phase might have a boundary that is narrow. Conversely, a broader boundary might exist between out-of-phase, i.e., "displaced" N $c(2\times2)$ patches. Yet, we must acknowledge that there is some calculational evidence now for slight rumpling for the same phase of N on the W(100) substrate.[53]

We now take up the issue as to whether any of the phonon mode energies can be influenced by compressive surface stress levels. In HAS experiments, we have explicitly looked for the influence of surface stress on the observable phonon modes. No measurable effects were seen: all phonon dispersion curves (mode energies) appear identical at exposure levels ranging from 90 to 5000 μC! In calculation, we find enormously softened or stiffened surface modes. However, these stiffenings/softenings do not occur for all surface phonon modes, but arise when a mode displays the dominant vertical vibration of first-layer Cu atoms or the dominant in-plane vibration of the first-layer Cu atoms that contract the N-Cu bond. The vertical mode softening is due mainly to the large expansion of the first layer, and the stiffening of the longitudinal modes derives mainly from the involvement of the N-Cu bond vibration. Thus, stiffening/softening of a phonon mode depends critically on the local coupling of N and Cu atoms. The stiffening/softening is not primarily due to the repulsive interaction between Cu atoms in the first layer (i.e., compressive surface stress), although it could still be contributing slightly.

V. SUMMARY

Rayleigh-type acoustic and optical modes of the $c(2\times2)$ N/Cu(001) phase have been measured with inelastic helium-atom scattering. Close agreement is found with our DFT slab calculations of vibrational modes in an optimized 0.5 ML N on Cu(001) structure. Our HAS measurements and DFT calculations also reproduce well the results of an earlier EELS measurement of the energy of a mode at the X-point (vertical displacement). The energy of this mode is insensitive to N addition. But calculations show that the character of this mode changes considerably as the surface unit cell is enlarged with local 0.5 ML N coverage. At the X point, both longitudinal and shear-horizontal motions combine in the displacement vectors of this, as well as in those of four other surface modes. The mode with the lowest energy at X is an optical clock mode: top-layer Cu atoms rotate about N positions. The energy calculated for this mode is 7.5 meV. The calculated energy of a shear-horizontal top-layer clean-surface mode lies very close, at 8.3 meV. Unfortunately, these modes are not observable with scattering probes.

Optical modes were detected, with HAS, along the [100] direction. N induces an $\sim$2.7 meV gap opening at the new Σ zone boundary. At the zone center, the optical mode is observed at 10.0 ± 0.3 meV. The calculated energy for this mode lies at 8.4 meV. This energy lies considerably below the analogous M point mode of the clean surface, at 16.8 meV. This mode softening is mainly due to the N-adsorbate-induced weakening of the first-to-second-layer binding which is compensated by increased in-plane interactions through binding to the N adsorbate. The mode softening, while dramatic, is not sufficient to induce a static rumpling of the topmost Cu layer, as was predicted by PhD results.

The N-containing surface shows no observable temperature- or coverage-induced variations in the vibrational modes. Stress levels internal to the N patches are known to vary considerably with N coverage.[24] The observed phonon modes are thus insensitive to lateral stress levels. The stiffening or softening in the calculation is specific to the local coupling of a phonon mode and is not primarily due to the compressive surface stress, i.e., to repulsive interactions of surface Cu atoms.

ACKNOWLEDGMENT

We thank Lyman Baker for critical reading of the manuscript. This work was supported in part under Grants No. CHE-0741423 and No. CHE-0718055 from NSF-USA.

*Present address: Department of Physics and Astronomy, University of Western Ontario, London, ON N6A 3K7.
†Corresponding authors.

[1] H. C. Zeng, R. N. S. Sodhi, and K. A. R. Mitchell, Surf. Sci. **188**, 599 (1987).
[2] H. C. Zeng and K. A. R. Mitchell, Langmuir **5**, 829 (1989).
[3] G. Prevot and B. Croset, Thin Solid Films **428**, 25 (2003).
[4] M. Sotto and B. Croset, Surf. Sci. **461**, 78 (2000).
[5] B. Croset, Y. Girard, G. Prévot, M. Sotto, Y. Garreau, R. Pinchaux, and M. Sauvage-Simkin, Phys. Rev. Lett. **88**, 056103 (2002).
[6] S. S. Dhesi, S. D. Barrett, A. W. Robinson, and F. M. Leibsle, Surf. Rev. Lett. **1**, 625 (1994).
[7] S. M. Driver and D. P. Woodruff, Surf. Sci. **492**, 11 (2001).
[8] F. Komori, S.-Y. Ohno, and K. Nakatsuji, Prog. Surf. Sci. **77**, 1 (2004).
[9] F. M. Leibsle, S. S. Dhesi, S. D. Barrett, and A. W. Robinson, Surf. Sci. **317**, 309 (1994).

[10] F. M. Leibsle, C. F. J. Flipse, and A. W. Robinson, Phys. Rev. B **47**, 15865 (1993).
[11] S.-Y. Ohno, K. Yagyuu, K. Nakatsuji, and F. Komori, Surf. Sci. **547**, L871 (2003).
[12] H. Ellmer, V. Repain, S. Rousset, B. Croset, M. Sotto, and P. Zeppenfeld, Surf. Sci. **476**, 95 (2001).
[13] M. V. Ngo, S. C. Avanzino, A. P. Marathe, and H. Ruelke, U.S. Patent No. 6599827 (2003).
[14] S.-Y. Ohno, K. Yagyuu, K. Nakatsuji, and F. Komori, Surf. Sci. **554**, 183 (2004).
[15] M. Getzlaff, M. Bode, and R. Wiesendanger, Acta Phys. Pol. A **104**, 327 (2003).
[16] F. Komori, S. Ohno, and K. Nakatsuji, J. Phys.: Condens. Matter **14**, 8177 (2002).
[17] K. Mukai, Y. Matsumoto, K. Tanaka, and F. Komori, Surf. Sci. **450**, 44 (2000).
[18] S. L. Silva and F. M. Leibsle, Surf. Sci. **440**, L835 (1999).
[19] T. M. Parker, L. K. Wilson, N. G. Condon, and F. M. Leibsle, Phys. Rev. B **56**, 6458 (1997).
[20] S.-Y. Ohno, K. Nakatsuji, and F. Komori, Surf. Sci. **523**, 189 (2003).
[21] K. D. Lee, T. Iimori, and F. Komori, Surf. Sci. **454-456**, 860 (2000).
[22] J. T. Hoeft, M. Polcik, M. Kittel, R. Terborg, R. L. Toomes, J. H. Kang, and D. P. Woodruff, Surf. Sci. **492**, 1 (2001).
[23] S. Hong, T. Rahman, E. Z. Ciftlikli, and B. J. Hinch (unpublished).
[24] Y. Yoshimoto and S. Tsuneyuki, Surf. Sci. **514**, 200 (2002).
[25] L. V. Goncharova, J. Braun, A. V. Ermakov, G. G. Bishop, D.-M. Smilgies, and B. J. Hinch, J. Chem. Phys. **115**, 7713 (2001).
[26] J. Ihm, A. Zunger, and M. L. Cohen, J. Phys. C **12**, 4409 (1979).
[27] S. Baroni, A. D. Corso, S. d. Gironcoli, and P. Giannozzi, http://www.pwscf.org
[28] D. Vanderbilt, Phys. Rev. B **41**, 7892 (1990).
[29] J. P. Perdew, K. Burke, and M. Ernzerhof, Phys. Rev. Lett. **77**, 3865 (1996).
[30] H. J. Monkhorst and J. D. Pack, Phys. Rev. B **13**, 5188 (1976).
[31] M. Methfessel and A. T. Paxton, Phys. Rev. B **40**, 3616 (1989).
[32] P. Giannozzi, S. de Gironcoli, P. Pavone, and S. Baroni, Phys. Rev. B **43**, 7231 (1991).
[33] S. Baroni, P. Giannozzi, and A. Testa, Phys. Rev. Lett. **58**, 1861 (1987).
[34] R. Franchy, Ber. Forschungszent. Juelich **2696**, 208 (1992).
[35] R. Franchy, M. Wuttig, and H. Ibach, Z. Phys. B: Condens. Matter **64**, 453 (1986).
[36] M. H. Mohamed and L. L. Kesmodel, Surf. Sci. Lett. **185**, L467 (1987).
[37] M. Wuttig, R. Franchy, and H. Ibach, Z. Phys. B: Condens. Matter **65**, 71 (1986).
[38] G. Benedek, J. Ellis, N. S. Luo, A. Reichmuth, P. Ruggerone, and J. P. Toennies, Phys. Rev. B **48**, 4917 (1993).
[39] R. Heid and K. P. Bohnen, Phys. Rep. **387**, 151 (2003).
[40] M. Alcántara Ortigoza, R. Heid, K. P. Bohnen, and T. S. Rahman, Phys. Rev. B **79**, 125432 (2009).
[41] A. Dal Corso, Phys. Rev. B **64**, 235118 (2001).
[42] V. Chis, B. Hellsing, M. Bernasconi, and J. P. Toennies, J. Phys.: Condens. Matter **19**, 305011 (2007).
[43] V. Chis, B. Hellsing, G. Benedek, M. Bernasconi, E. V. Chulkov, and J. P. Toennies, Phys. Rev. Lett. **101**, 206102 (2008).
[44] V. Higgs, P. Hollins, M. E. Pemble, and J. Pritchard, J. Electron Spectrosc. Relat. Phenom. **39**, 137 (1986).
[45] T. S. Rahman and H. Ibach, Phys. Rev. Lett. **54**, 1933 (1985).
[46] H. Ibach, J. E. Mueller, and T. S. Rahman, Philos. Trans. R. Soc. London **318**, 163 (1986).
[47] J. E. Müller, M. Wuttig, and H. Ibach, Phys. Rev. Lett. **56**, 1583 (1986).
[48] S. M. Driver, J. T. Hoeft, M. Polcik, M. Kittel, R. Terborg, R. L. Toomes, J. H. Kang, and D. P. Woodruff, J. Phys.: Condens. Matter **13**, L601 (2001).
[49] S. M. Driver and D. P. Woodruff, Surf. Sci. **539**, 182 (2003).
[50] T. E. Wofford, S. M. York, and F. M. Leibsle, Surf. Sci. **539**, 186 (2003).
[51] T. E. Wofford, S. M. York, and F. M. Leibsle, Surf. Sci. **522**, 47 (2003).
[52] C. F. Hirjibehedin, C. P. Lutz, and A. J. Heinrich, Science **312**, 1021 (2006).
[53] A. Michaelides, P. Hu, M. H. Lee, A. Alavi, and D. A. King, Phys. Rev. Lett. **90**, 246103 (2003).